International Journal of Pharmaceutics: X 4 (2022) 100119

Contents lists available at ScienceDirect

International Journal of Pharmaceutics: X

journal homepage: www.sciencedirect.com/journal/international-journal-of-pharmaceutics-x

Preparation, characterization, and pharmacokinetics of rivaroxaban cocrystals with enhanced in vitro and in vivo properties in beagle dogs

Yuanyuan Meng [a,b], Fangyun Tan [a,b], Jiaxin Yao [a], Yanan Cui [a], Yumiao Feng [a,c], Zhiping Li [a], Yuli Wang [a], Yang Yang [a], Wei Gong [a,*], Meiyan Yang [a,*], Xiaolong Kong [b], Chunsheng Gao [a]

[a] State Key Laboratory of Toxicology and Medical Countermeasures, Beijing Institute of Pharmacology and Toxicology, Beijing 100850, China
[b] School of Pharmacy, Guangxi Medical University, Nanning 530000, China
[c] Pharmaceutical College, Henan University, Kaifeng 475001, China

ARTICLE INFO

Keywords:
Cocrystals
Rivaroxaban
Beagle dogs
Dissolution
Solubility
Permeation
Pharmacokinetics

ABSTRACT

Rivaroxaban (RIV) is a direct Factor Xa inhibitor anticoagulant, but the oral bioavailability of RIV is estimated to be only 60% due to its poor solubility. The aim of the present study was to improve the solubility and bioavailability of RIV. Five cocrystals—p-hydroxybenzoic acid (HBA), 2,4-dihydroxybenzoic acid (DBA), nicotinamide (NA), isonicotinamide (IA), and succinic acid (SA)—were used as cofomers and were successfully obtained and characterized by powder X-ray diffraction, thermal analysis, and Fourier transform infrared spectra. RIV-DBA and RIV-HBA cocrystals showed obvious improvements in solubility, dissolution (under sink conditions), and intrinsic dissolution rates versus RIV. Moreover, the dissolution of RIV-HBA, RIV-DBA, and RIV-SA cocrystals under non-sink conditions showed obvious "spring and parachute" patterns. The in vitro permeability levels in a Caco-2 cell model of RIV-DBA and RIV-IA cocrystals were significantly improved versus RIV. Pharmacokinetic studies in beagle dogs showed that RIV-DBA and RIV-HBA cocrystals had higher bioavailability than RIV. The enhancements in solubility and bioavailability indicate the potential of RIV cocrystals as a better candidate for the treatment of thrombosis versus RIV.

1. Introduction

The global mortality rate of cardiovascular diseases is greater than one-third of reported human cases (Al-Mallah et al., 2018). Thrombosis is a contributory factor in cardiovascular disease, and anticoagulation therapy is one of the most widely used clinically preventive treatments of thrombotic diseases (Abadie et al., 2020; Boban et al., 2016). Rivaroxaban (RIV) is a direct Factor Xa inhibitor and is commonly used both to prevent and to treat venous thrombosis for its effective and convenient anticoagulant options (Boban et al., 2016; Wingert et al., 2018; Young et al., 2020). Versus the traditional anticoagulant warfarin, the advantages of RIV are its rapid onset of action and comparatively few drug interactions and side effects (Weitz et al., 2020; Xue et al., 2018). However, RIV is an un-ionized neutral molecule with low and pH-independent solubility. It suffers from poor oral bioavailability, as low as 60% at the 20 mg dose under fasting conditions (Bae et al., 2019; Demir et al., 2020; Takács-Novák et al., 2013; Xue et al., 2018). The bioavailability of RIV is dose-dependent (100% for 5 mg dosage, 90% for 10 mg dosage, and 60% for 20 mg dosage) (Demir et al., 2020). This low bioavailability due to low solubility leads to problems such as increased variations between fasting and fed conditions, delayed effect, and failure to achieve dose proportionality.

It is important to improve the oral bioavailability of RIV to reduce dosing frequency and thus to improve patient compliance. Recently, several techniques have been utilized to improve the solubility and bioavailability of RIV such as cocrystals (Kale et al., 2020), amorphous solid dispersions (Metre et al., 2018), microemulsions (Wingert et al., 2018), self-nanoemulsifying drug delivery system (Xue et al., 2018), and micelles (Cao et al., 2016). Among these strategies, cocrystals have attracted great interest and are a promising strategy to modify the physical-chemical properties of solid-state materials. Cocrystals can improve mechanical properties and enhance the in vivo bioavailability of poorly water-soluble drug. This can generate and extend intellectual property (Elder et al., 2013; Karimi-Jafari et al., 2018; Wong et al., 2021).

Pharmaceutical cocrystals are defined as a solid single-phase crystal

* Corresponding authors.
E-mail addresses: usnitro2004@126.com (W. Gong), ymyzi@163.com (M. Yang).

https://doi.org/10.1016/j.ijpx.2022.100119
Received 10 February 2022; Received in revised form 4 May 2022; Accepted 19 May 2022
Available online 21 May 2022

containing active pharmaceutical ingredient (API) and coformers bound with each other by non-covalent interactions in a defined stoichiometric ratio under ambient conditions (Cavanagh et al., 2020). This new crystalline form provides a feasible method to adjust the physicochemical properties without changing the chemical structure of the API (Childs et al., 2013; Sathisaran and Dalvi, 2018). In recent decades, great efforts have been made to improve solubility, permeability, or bioavailability of poorly water-soluble drugs by inserting a more soluble coformer in the crystal lattice leading to a reduced solvation barrier (Cysewski, 2018; Dalpiaz et al., 2018; Liu et al., 2016; Wen et al., 2005). Cocrystals can also enhance membrane permeation and diffusion due to the induced supersaturated drug concentration (Ferretti et al., 2015; Guo et al., 2018; Liu et al., 2020b).

RIV is a Biopharmaceuticals Classification System (BCS) Class II drug with low oral bioavailability (Kushwah et al., 2021). Rivaroxaban-malonic acid cocrystal (RIV-MAL) could improve the tabletability and increase the water sorption of RIV (Kale et al., 2020; Kale et al., 2019). However, to the best of our knowledge, the study and application of improved permeability and bioavailability of RIV by cocrystals has not yet been reported (Grunenberg et al., 2011). In addition, although some progress has been made in the design and preparation of cocrystals, information on in vivo pharmacokinetics, especially in beagle dogs, is still lacking and needs further study (Cho et al., 2021; Yang et al., 2022).

The goal of this study was to enhance the physicochemical properties and oral bioavailability of poorly water-soluble RIV. RIV have amino and carbonyl functional groups in the structure, and thus components with hydroxyl, carbonyl and amino functional groups can form hydrogen bonds with RIV, e.g., p-hydroxybenzoic acid (HBA), 2,4-dihydroxybenzoic acid (DBA), nicotinamide (NA), isonicotinamide (IA), and succinic acid (SA). These five were chosen as cocrystal coformers (CCF) according to the supramolecular synthon principles. The chemical structures of the RIV, HBA, DBA, NA, IA, and SA are shown in Fig. 1. The resulting RIV cocrystals were verified using powder X-ray diffractometry (PXRD), differential scanning calorimetry (DSC), Fourier transform infrared spectroscopy (FTIR), and scanning electron microscopy (SEM). The effect of surfactant SDS on the solubility and dissolution of five cocrystals under sink and non-sink conditions were then investigated. Moreover, we investigated the permeation behavior across Caco-2 cell monolayers (Kamiloglu et al., 2015; Wallace et al., 2014) (employed as an in vitro model of human intestinal epithelial barrier) of RIV, its cocrystals, and its physical mixtures (PMs). Finally, the pharmacokinetics in beagle dogs of two preferred cocrystals (RIV-DBA and RIV-HBA) were compared with pure RIV and PMs.

2. Materials and methods

2.1. Materials

Rivaroxaban (RIV) was purchased from Meilun Biotech Co., Ltd. (Dalian, China). Coformers such as p-hydroxybenzoic acid (HBA), 2,4-dihydroxybenzoic acid (DBA), nicotinamide (NA), isonicotinamide (IA), and succinic acid (SA) were all purchased from Sinopharm Chemical Reagent Co., Ltd. (Shanghai, China). Sodium dodecyl sulphate (SDS) was purchased from VMR International Inc. (Pennsylvania, UK). Acetonitrile was applied by Sigma-Aldrich Co., Ltd. (St. Louis, MI, USA). Double distilled freshly water was used for the whole study. All of the other reagents were analytical grade, purchased from commercial suppliers.

Human colon carcinoma cells (Caco-2) were supplied by the Cell Resource Centre of IBMS (Beijing, China). The male beagle dogs (9.0 ± 1.2 kg) were purchased from Marshall Co., Ltd. (permit number: SCXK (Jing) 2021–0002, Beijing, China).

2.2. HPLC analysis

The RIV concentrations were simultaneously analyzed by a Waters HPLC system composed of a Waters 2695 Separation Module, a Waters 2487 Dual λ Absorbance Detector, and a Waters Empower 2 Workstation. The HPLC analysis conditions were as follows: ZORBAX SB C18 column (5 μm, 4.6 mm × 250 mm, Agilent, Santa Clara, CA, USA); column temperature, 30 °C; mobile phase, acetonitrile-water (60/40, *v*/v); flow rate, 1.0 ml/min; wavelength, 250 nm; injection volume, 20 μl, the retention time of RIV of raw API and cocrystal samples were both about 5.26 min.

2.3. Preparation of cocrystals and physical mixture

Three organic acids (HBA, DBA, and SA) and two organic bases (NA and IA) were chosen as coformers. The RIV cocrystals were prepared by liquid-assisted grinding. A 1:1 M ratio of RIV and the above-mentioned coformers were dissolved in drops of ethanol in a agate mortar and pestle and then ground for 30 min. The resulting solid phases were vacuum dried overnight and then characterized by PXRD and DSC. To decrease the influence of particle size, the samples were passed through an 80-mesh sieve before the experiment.

A physical mixture (PM) of RIV and coformer were prepared by gently mixing at a drug-to-coformer ratio of 1:1 (mmol/mmol) for 10 min in a plastic bag. To decrease the influence of particle size, the samples were passed through an 80-mesh sieve before the experiment.

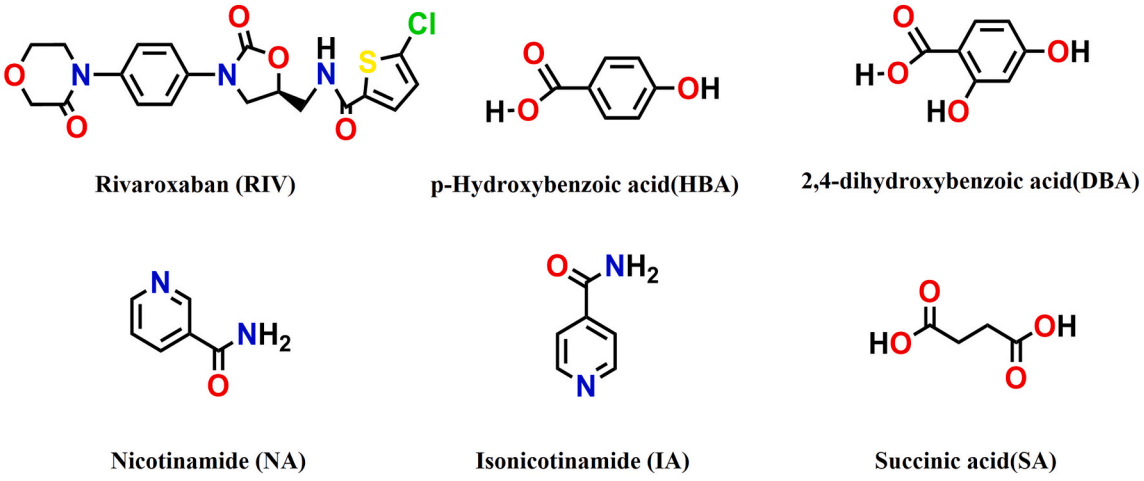

Fig. 1. Molecular structure of rivaroxaban (RIV), 4-hydroxybenzoic acid (HBA), 2,4-dihydroxybenzoic acid(DBA), nicotinamide (NA), Isonicotinamide (IA), and succinic acid(SA).

2.4. Characterization of cocrystals

2.4.1. PXRD

The diffraction patterns of solid samples were recorded using X-ray diffractometer (Bruker XRD-D8 Advance, Karlsruhe, Germany) equipped with Cu as the anode material using a tube current of 40 mA and a tube voltage of 40 kV. The samples were continuously scanned from 5° to 50° (2θ) at a scanning rate of 0.2°/min.

2.4.2. Thermal analyses

DSC measurements were conducted using a TA Q200 DSC instrument (New Castle, DE, USA) with 10 °C/min heating rate. The samples were heated in a sealed aluminum pan from 0 °C to 250 °C. An empty aluminum pan was used as a reference.

Thermogravimetric analysis (TGA) measurements were conducted on a TGA 8000 equipment (Waltham, MA, USA) with 10 °C/min heating rate. Approximately 5 mg samples were weighed and placed in the alumina crucibles, and the temperature range was set from 0 °C to 250 °C.

2.4.3. SEM

A scanning electron microscope (Hitachi S-4800, Tokyo, Japan) was used to study the morphological characteristics of solid samples. The powder was stuck to a brass stub by double side adhesive tape and then vacuum-coated with a layer of gold to make it electrically conductive. The samples were examined at an accelerating voltage of 15 kV.

2.4.4. FTIR

An FTIR spectrophotometer (Nicolet 6700, Waltham, MA, USA) was used in the diffuse reflectance mode to evaluate the spectra of solid samples. The samples were mixed well with potassium bromide (approximately 1:50, weight ratio) in an agate mortar and compressed with a tablet-pressing machine. The prepared tablets were scanned from 4000 to 400 cm^{-1} after collecting the background spectrum. The signal changes of the samples were compared to analyze the interactions between them.

2.5. Solubility measurements

To study the solubility of RIV cocrystals with HBA, DBA, NA, IA, and SA as corresponding coformers, solubility testing used a magnetic-stirring method. Excess samples were added to a small vial containing 30 ml of water or SDS solutions at 0.2% and 0.4% (*w/v*) levels and then stirred at 37 °C and 120 rpm for 24 h. Aliquots were filtered through 0.45-μm filters and diluted properly to determine the concentrations of RIV by high-performance liquid chromatography (HPLC) as described above. Solubility testing of pure drug and physical mixtures under the same conditions were also conducted as a comparison. All experiments were carried out in triplicate. The solid residues retrieved from the solubility tests were dried and analyzed by PXRD and DSC.

2.6. Dissolution under sink conditions

Powder dissolution under sink conditions used the paddle method with a Dissolution Tester (TIANDA TIANFA ZRS-8G, Tianjin, China). Pure RIV, PMs, and cocrystals were added to water and SDS solutions at 0.2% and 0.4% level, separately. The volume of dissolution media was 900 ml to achieve sink conditions with a paddle speed of 100 rpm at 37 °C. Samples (3 ml) were taken at 5, 10, 15, 20, 30, 45, 60, 90, 120, 180, 240, and 300 min, and an equal volume of fresh medium was added to maintain a constant dissolution medium volume. The samples were filtered through 0.45-μm filters and diluted properly for determination of the concentrations of RIV by HPLC as described above. The dissolution profiles were represented as the cumulative percentages of the amount of the drug released at each sampling interval. All experiments were carried out in triplicate.

2.7. Dissolution under non-sink conditions

Powder dissolution under non-sink conditions is commonly used to mimic the in vivo conditions of supersaturated cocrystals with "spring and parachute" patterns (Hu et al., 2019; Liu et al., 2016). Pure RIV and an equivalent of cocrystals were added to 50 ml of water. The dissolution experiments were performed at 37 °C with magnetic stirring at 120 rpm (IKA ICC control IB R RO 15eco, IKA-Werke GmbH & Co. KG, Staufen, Germany). Samples (1 ml) were withdrawn at specified time intervals (5, 10, 15, 20, 30, 45, 60, 90, 120, 180, 240, 300, and 360 min), immediately filtered through 0.45 μm filters, and then diluted properly to determine the concentrations of dissolved RIV by HPLC as described above. All experiments were carried out in triplicate. The solid residues retrieved from the water non-sink dissolution tests were dried and analyzed by PXRD, DSC, and SEM.

2.8. Intrinsic dissolution test

The intrinsic dissolution rate (IDR) measurements used a 708-DS Dissolution Apparatus (Agilent Technologies, Santa Clara, CA, USA) via the rotating disc method. Approximately 100 mg of solid sample was compressed to a disk using a hydraulic press at 10 MPa for 1 min with a 7.98-mm-diameter die. The disk was sealed with paraffin wax, thus providing a flat surface on one side for dissolution. The disk was then immersed in 900 ml of the dissolution medium (pH 1.2 HCl solution at 37 °C) with the disk rotating at 250 rpm. At each time interval (5, 10, 15, 20, 30, 45, 60, 90, and 120 min), 3 ml of the dissolution medium was withdrawn and replaced by an equal volume of fresh medium to maintain a constant volume. Samples were filtered and properly diluted. The concentrations of RIV were determined via HPLC. All tests were performed in triplicate.

2.9. Permeation studies

2.9.1. Caco-2 cell culture

Caco-2 cell wells were used as an in vitro absorption model to investigate the penetration of the cocrystals. Caco-2 cells were stored in an incubator at 37 °C with 95% relative humidity and 5% CO_2 atmosphere. The Caco-2 cell line was grown and differentiated to cell monolayers in 24-well trans well chambers (Corning, NY, USA). To summarize, Caco-2 cells were seeded onto the upper chamber of cell culture inserts (0.4 μm) at a density of 5×10^4 cells per well, and the trans endothelial electrical resistance (TEER) of the cell membrane was recorded. At 21 days post-seeding, the cells developed TEER values over 300 Ω•cm^2 (Tran et al., 2020).

2.9.2. In vitro cytotoxicity

A Cell Counting Kit-8 (CCK-8) was used to determine the inhibitory effect of RIV cocrystals and physical mixtures of drug and coformers on Caco-2 cell proliferation (Cai et al., 2019). Logarithmic phase Caco-2 cells were collected and 5000 cells were seeded and differentiated in 96-well plates at 37 °C in a 5% CO_2 atmosphere. Different drug solutions containing 10, 50, 100, 250, or 500 μg/ml of RIV were added to each group. After 48 h of culture, 96-well plates were washed three times with pre-warmed PBS before studies, and then 20 μl of CCK-8 solution was added to each well and incubated for 2 h. The absorbance of each well was measured at 450 nm using a plate reader (Tecan Spark, Austria). The relative cell viability (%) was calculated by comparing the absorbance of the treated cells with controls.

2.9.3. Permeability calculation

The in vitro cell monolayers absorption model was established next. Before permeability studies, Caco-2 cell monolayers were washed three times with pre-warmed HBSS. The experiments were initiated by adding 0.5 ml of the test solution to the apical chamber and 1.0 ml of HBSS to the basolateral chamber. Samples (100 μl) were then taken from the

basolateral chamber and immediately replaced with the same volume of HBSS at 37 °C and predetermined time intervals of 120 min. The samples were stored at −20 °C until analysis. The concentration of RIV in the transport buffer samples was determined using HPLC analysis. The apparent permeability coefficient (P_{app}) across the Caco-2 cell monolayer was calculated according to the following equation: $Papp = (dQ / dt) / (A C_0)$ where P_{app} is the apparent permeability coefficient in cm/min, dQ / dt (μg/min) is the transport rate, A is the surface area of the monolayer (1.13 cm^2), and C_0 is the initial concentration of RIV (250 μg/ml).

2.10. Pharmacokinetic (PK) studies in beagle dogs

2.10.1. Drug administration and blood sampling

The dog pharmacokinetic study was approved (approval number IACUC-DWZX-2021-593) by the Animal Care and Use Ethics Committee of the Beijing Institute of Pharmacology and Toxicology (Beijing, China). The dogs were kept in a temperature-controlled environment with 12-h light/12-h dark cycle for six days. A crossover pharmacokinetic study was carried out in beagle dogs ($n = 6$) to evaluate the in vivo performance of different formulations. RIV, PMs, and cocrystal-based formulations were administered orally at 2 mg/kg. The dogs were fasted overnight prior to each dosing session and were given food again 4 h after dosing. Oral administration of formulations was followed immediately by 50 ml of water. A washout period of 7 days was used between dosing. Blood samples (2 ml) were withdrawn from the cephalic *v*ein and collected in heparinized tubes at 0.17, 0.5, 1, 1.5, 2, 2.5, 3, 4, 6, 8, 12, and 24 h after dosing and subsequently centrifuged at 5000 *g* for 10 min at 4 °C. The harvested plasma was stored at −80 °C until HPLC-MS/MS analysis.

2.10.2. Blood sample analysis

Plasma samples were thawed at room temperature prior to use. Aliquots of plasma (100 μl) were vortex-mixed for 5 min with 100 μl internal standard (diphenhydramine, 500 ng/ml in acetonitrile) and 300 μl acetonitrile. The mixture was centrifuged at 14000 *g* for 5 min and filtered through a membrane filter (0.45 mm). The filtrate was then analyzed by HPLC-MS/MS method.

2.10.3. HPLC-MS/MS analysis

Analysis of RIV concentrations in plasma used an Agilent HPLC with electrospray ionization and tandem mass spectrometry detection (Pump G1312C, Autosampler 1367E, Degasser G1322A, G6460A triple quad mass spectrometer, Agilent Technologies, Santa Clara, CA, USA). Diphenhydramine was used as the internal standard (IS). The analysis conditions of HPLC-MS/MS included a reversed phase C18 analytical column (3.5 μm, 2.1 mm - 100 mm, Agilent, Santa Clara, CA, USA) and gradient elution conditions at a flow rate of 0.3 ml/min. The mobile phase was acetonitrile- 0.1% formic acid solution (30/70, *v*/v). The triple-quadrupole mass spectrometer was operated in negative ionization mode, and detection and quantification used multiple-reaction monitoring (MRM). Tandem mass spectrometry (MS/MS) detection was conducted by monitoring the fragmentation of 436.0 → 144.8 (*m/z*) for RIV and 256.2 → 167.2 (m/z) for IS. The productions were generated with a collision energy of 28 eV.

2.10.4. Pharmacokinetic analysis

A noncompartmental model was used to fit the pharmacokinetic analysis results of pure RIV, cocrystals, and PM. The maximal values for drug concentration and time were C_{max} (ng/ml) and t_{max} (h), respectively. The area under the plasma concentration-time curve up to the last sampling time was calculated as the AUC_{0-t} (ng/ml ·h) using a linear trapezoidal rule. The $AUC_{0\sim\infty}$ (ng/ml ·h) could also be calculated according to the formula $AUC_{0\sim\infty} = AUC_{0\sim t} + C_{t/k}$, where C_t was the measured concentration at time t, and k was the terminal elimination rate constant estimated by log-linear regression analysis. An apparent terminal elimination half-life ($t_{1/2}$) was obtained from $t_{1/2} = 0.693/k$. The relative bioavailability (f_{rel}) could be derived as $(AUC_T/AUC_R) \times 100\%$.

2.11. Statistical analysis

All data were presented as means ± standard deviation (SD) and pharmacokinetic data were calculated by Drug and Statistics (DAS) 2.0 software. The statistical significance of dissolution profiles were analyzed by one-way variance analysis (ANOVA) (significance level of 0.05) and a multiple post-hoc Tukey's test using SPSS19.0 software (IBM Corp., Armonk, NY, USA).

3. Results and discussions

3.1. Characterization of RIV cocrystals

3.1.1. PXRD

PXRD is a commonly used and a powerful tool to characterize the formation of cocrystals. The crystalline state of the starting materials of RIV and CCFs, PMs, and RIV cocrystals are presented in Fig. 2a. The RIV and CCFs (HBA, DBA, SA, NA and IA) displayed a series of intense peaks, thus demonstrating their crystalline character. The RIV/CCF PMs showed all major peaks from RIV and CCFs at various diffraction angles, which suggested that the crystallinity of the drug and coformers remained unchanged in the physical mixture. The RIV-HBA cocrystals exhibit new characteristic interference peaks at 2θ at 9.1° and 27.2°; RIV peaks at 2θ angles such as 16.6° and 26.7° disappeared (Fig. 2a-1). The RIV-DBA cocrystals exhibit new characteristic interference peaks at 2θ at 14.3° and 24.9°, and RIV peaks at 2θ angles such as 22.6° and 26.7° disappeared (Fig. 2a-2). The RIV-NA cocrystals exhibit new characteristic interference peaks at 2θ at 20.6° and 24.6°, and RIV peaks at 2θ angles such as 16.6° and 26.6° disappeared (Fig. 2a-3). The RIV-IA cocrystals exhibit new characteristic interference peaks at 2θ at 15.5° and 27.8°, and RIV peaks at 2θ angles such as 16.6° and 22.6° disappeared (Fig. 2a-4). The RIV-SA cocrystals exhibit new characteristic interference peaks at 2θ at 20.7° and 25.2°, and RIV peaks at 2θ angles such as 22.6° and 26.7° disappeared (Fig. 2a-5). The PXRD pattern of the five cocrystals displayed characteristic profiles that were different from the characteristic peaks of the drug and coformers, thus suggesting the formation of a new crystalline phase.

3.1.2. Thermal analyses

The physicochemical status information such as melting, decomposition, or changes in the heat capacity of the drug dispersed in other material could be provided using thermal analyses. Analysis of TGA curves of RIV and coformers (Fig. S1) reveals that there is no mass loss before the melting event, indicating their unsolvated properties. Fig. 2b shows the DSC thermal behavior of samples. RIV shows a sharp endothermic peak attributed to the melting point at 231.7 °C, which indicated a crystalline structure. HBA, DBA, NA, IA, and SA were characterized by a melting point at 216.4 °C, 208.3 °C, 133.0 °C, 160.2 °C, and 187.2 °C, respectively. RIV-HBA, RIV-DBA, RIV-NA, RIV-IA, and RIV-SA cocrystals displayed a sharp peak at 174.3 °C, 171.7 °C, 158.4 °C, 84.7 °C, and 125.8 °C (Fig. 2b), which confirmed crystalline structures. However, the final identification and verification of the cocrystals formation were concluded via various significant changes in characteristics and signature peaks during spectroscopy.

3.1.3. FTIR

FTIR spectroscopy offered information on the changes in the bonding between functional groups. The RIV, CCF, PMs, and its cocrystals were also analyzed by FTIR spectroscopy to obtain evidence of noncovalent interactions (Fig. 2c). RIV had characteristic absorption bands of amide at 3353.41 cm^{-1} for ν_{N-H}, 1667.21 cm^{-1} for $\nu_{C=O}$, and 1644.88 cm^{-1} for β_{N-H}; –C=O stretching occurred at 1736.78 cm^{-1}, and –C=C stretching

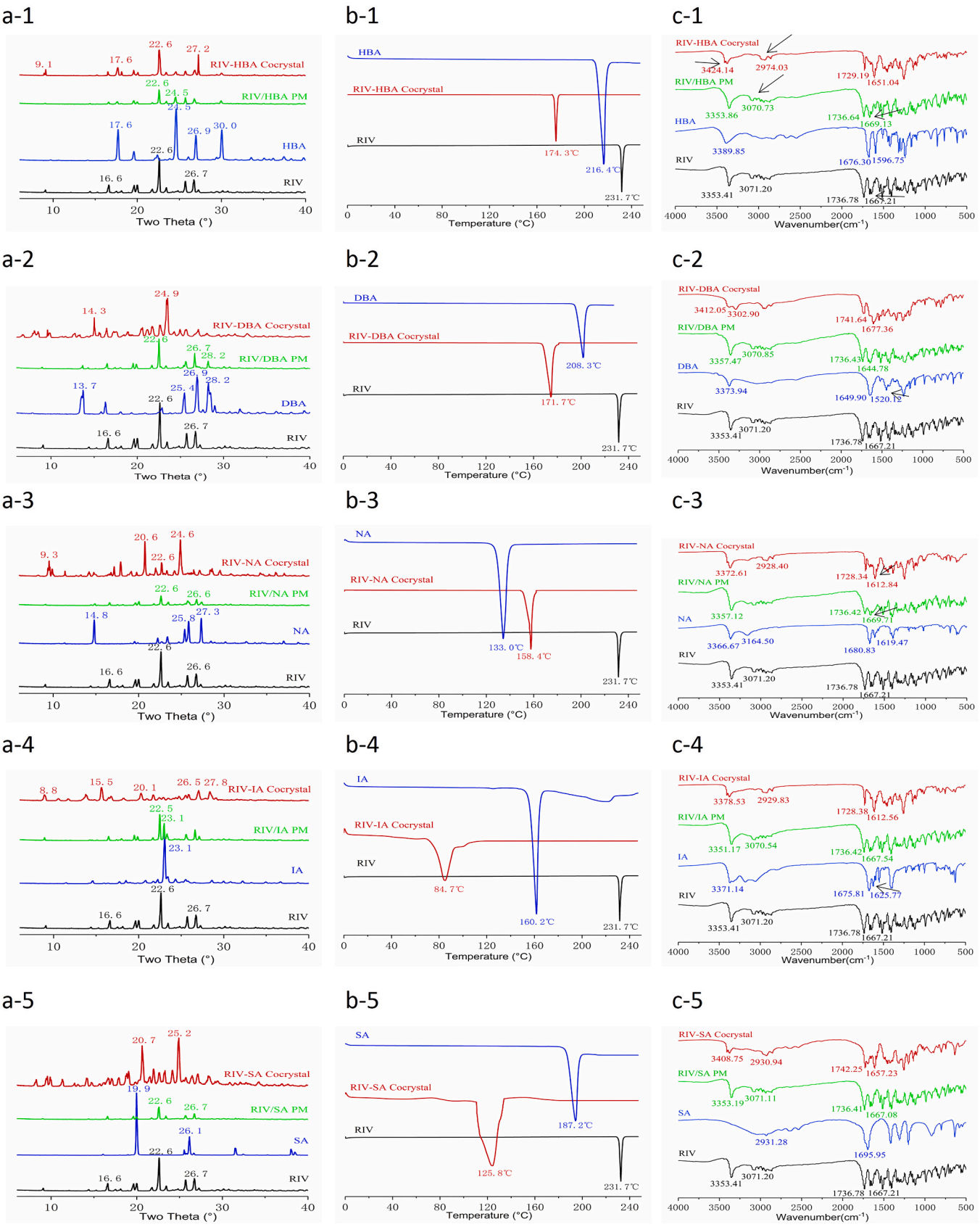

Fig. 2. PXRD (a), DSC (b), and FTIR (c) patterns of RIV-HBA(1), RIV-DBA(2), RIV-NA(3), RIV-IA(4), and RIV-SA(5). RIV: black curve, coformers: blue curve, PM: green curve, cocrystals: red curve. (For interpretation of the references to colour in this figure legend, the reader is referred to the web version of this article.)

of an aromatic ring was seen at 1517.02 cm^{-1}. The RIV-HBA cocrystal data is shown in Fig. 2(c-1): The –C=O stretching of RIV shifted from 1667.21 to 1651.04 cm^{-1}, and the oxhydryl group vibration signals of HBA shifted from 3389.85 to 2974.03 cm^{-1}. These shifted to low wavenumbers versus RIV and HBA. These shifts of wavenumber indicate that the new molecular interactions of RIV-HBA significantly influence the functional group positions. For RIV-DBA cocrystal (Fig. 2c-2), the IR result differs obviously from both starting materials. The stretching vibration of the oxhydryl group presents two sharp peak at 3412.05 and 3302.90 cm^{-1}. Compared with the starting materials, they shift to high wavenumber zone. For RIV-NA cocrystal (Fig. 2c-3), the carbonyl group vibration signals of RIV shifted from 1667.21 to 1612.84 cm^{-1}, and the amino stretching of NA shifted from 3366.67 to 3372.61 cm^{-1}. For RIV-IA cocrystal, the carbonyl group vibration signals of RIV shifted from 1667.21 to 1612.56 cm^{-1}, and the amino stretching of IA shifted from 3371.14 to 3378.53 cm^{-1} (Fig. 2c-4). For RIV-SA cocrystal (Fig. 2c-5), the amide, carbonyl and oxhydryl groups can be assigned at 3408.75 cm^{-1}, 1657.23 cm^{-1}, and 2930.94 cm^{-1}, respectively. The wavenumbers shift significantly versus RIV and SA. These IR absorption shifts of the five investigated cocrystals, indicate that intermolecular interactions of each cocrystal are the main forces to influence the IR wavenumbers.

3.1.4. SEM

SEM can visualize the observation of morphology such as the surface and crystal structures of solid samples (Tian et al., 2006). Microstructures of RIV, HBA, DBA, NA, IA, and SA are shown in Fig. S2. The morphology of RIV included regular flaky crystals; HBA appeared as prismatic crystals, DBA appeared as angular crystals, NA and SA were spherical granular crystals, and IA mostly had columnar crystals accompanied by large lumps with obvious crystal characteristics. Overall, PXRD, and DSC suggested the formation of five novel RIV-DBA, RIV-HBA, RIV-SA, RIV-IA, and RIV-NA cocrystals. The FTIR results indicated H-bonding between the drug and coformers.

3.2. Solubility study

The solubility of RIV, PMs, and cocrystals in water and solutions with different levels of SDS (0.2%, 0.4%, *w/v*) are shown in Fig. 3. In water, the solubility of RIV-DBA, RIV-HBA and RIV-SA cocrystals increased versus pure RIV while the solubility of RIV-NA and RIV-IA cocrystals decreased. Moreover, the solubility of the RIV-DBA cocrystal was significantly higher than that of the other four cocrystals in water presenting at least a 9.0-fold increase (Fig. 3b). There were no significant changes in the solubility of five PMs versus pure RIV (Fig. 3a).

Surfactants such as SDS could be used to maintain supersaturation of cocrystals based on micellar solubilization mechanisms; this has been

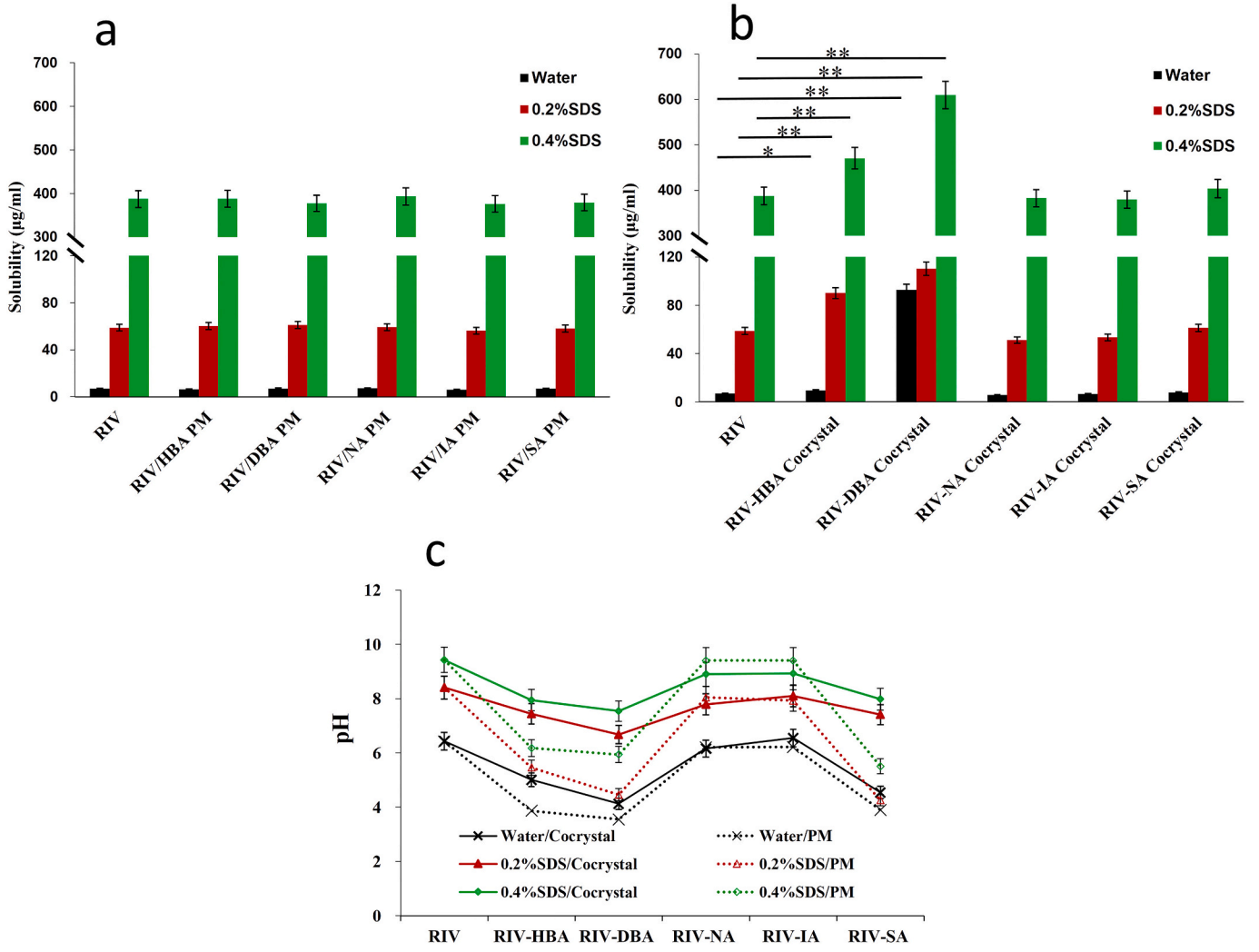

Fig. 3. Solubility of RIV from single components. PMs (a) and its cocrystals (b) in water and SDS solutions at 0.2% and 0.4% (*w/v*) levels ($n = 3$). *$P < 0.05$, **$P < 0.01$, compared to RIV. (c) The pH values of the bulk media solutions after solubility testing (mean ± SD, n = 3).

shown in previous study (Childs et al., 2013; Feng et al., 2021). Therefore, the effect of SDS on the solubility of RIV cocrystals was also studied here. The critical micelle concentration (CMC) of SDS is 0.24% (w/v) at 298 K (Ruiz-Morales and Romero-Martinez, 2018). In pure RIV, a good linear relationship was obtained between the SDS levels (w/v) and the RIV solubility when the concentration of SDS is above the CMC (data not shown). The solubility of both RIV cocrystals and PMs were improved with increasing SDS concentrations. The drug solubility ranked from highest to lowest as follows: RIV-DBA > RIV-HBA > RIV-SA > RIV > RIV-NA > RIV-IA cocrystals; there was no significant difference between RIV and their parent physical mixtures.

Good et al. stated that the solubility of a cocrystal cannot be accurately measured for highly soluble cocrystals because they can transform to the most stable drug form in solution (Good and Rodríguez-Hornedo, 2009). For a metastable cocrystal, the drug concentration associated with the cocrystal solubility is greater than the solubility of the stable drug form. Cocrystallization cannot always improve the solubility of poorly water-soluble drugs, and cocrystal dissociation is one possible reason. To investigate the possible mechanism, the pH of the bulk media solutions were also measured after solubility testing (Fig. 3c). The pH values of cocrystals in water from high to low were RIV-IA > RIV > RIV-NA > RIV-HBA > RIV-SA > RIV-DBA; this rank did not change in SDS solution. The solubility of cocrystals showed no obvious relationship with the pH values of the bulk media, which were produced by the coformers. This might be because of the pH-independent solubility of RIV—a non-ionizable drug (Kushwah et al., 2021). The PXRD and DSC results of residual solids after solubility test are shown in Fig. S3. For pure RIV, PMs, as well as cocrystals of RIV-HBA, RIV-DBA, RIV-NA, and RIV-SA, the precipitation of RIV were observed. However, for RIV-IA cocrystal, the supersaturation was maintained over 24 h.

3.3. Powder dissolution under sink and non-sink conditions

To predict the in vivo absorption behavior of cocrystals, it is important to study the dissolution pattern especially for BCS II drugs with a dissolution rate-limited absorption pattern (Childs et al., 2013; Zhou et al., 2020). Powder dissolution under sink conditions is commonly used to compare drug dissolution, while non-sink conditions

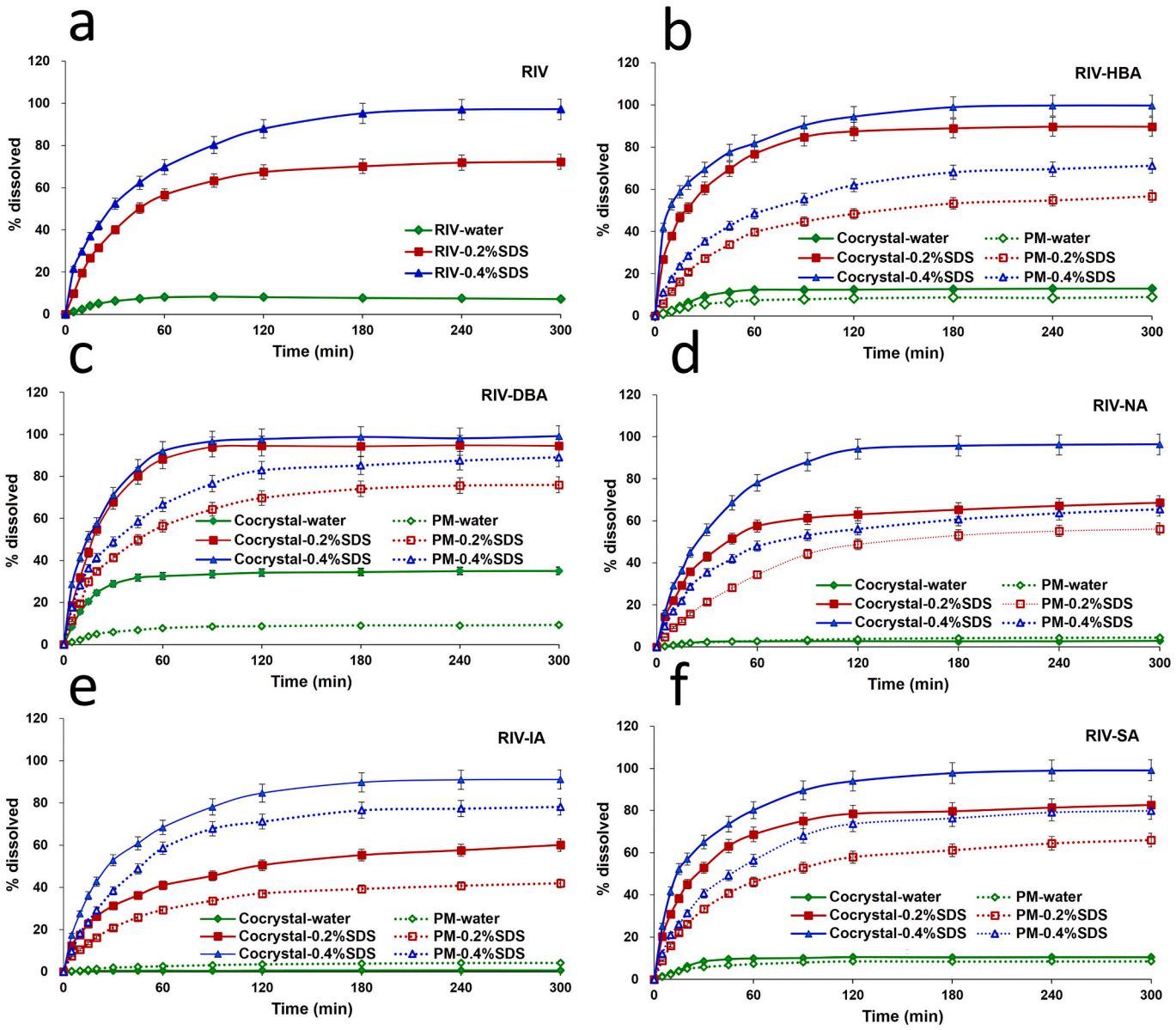

Fig. 4. Powder dissolution profiles of RIV(a), RIV-HBA (b), RIV-DBA (c), RIV-NA (d), RIV-IA (e), and RIV-SA (f) in water and SDS solutions at 0.2% and 0.4% (*w/v*) levels under sink conditions (mean ± SD, $n = 3$).

are usually conducted to study the supersaturation state in solution (Childs et al., 2013). Considering the CMC value, the SDS used in the dissolution test had the same level as the solubility test, i.e., 0.2% and 0.4% (*w/v*). The dissolution profiles of samples in water and solutions with 0.2% and 0.4% (w/v) SDS under sink and non-sink conditions are shown in Figs. 4 and 5, respectively.

Fig. 4 shows that drug dissolution of pure RIV, PMs, and cocrystals all increased with increasing SDS level. In water and solution with 0.2% SDS, the drug dissolution ranked from highest to lowest as follows: RIV-DBA > RIV-HBA > RIV-SA > pure RIV > RIV-NA > RIV-IA cocrystals. These were consistent with the previous RIV solubility results, thus suggesting the solubility-limited dissolution patterns of poorly water-soluble RIV. However, in a solution with 0.4% SDS, there were no significance differences among drug and cocrystals. The physical mixture of the drug and coformers showed lower dissolution than cocrystals due to the pH-independent solubility pattern of RIV(Takács-Novák et al., 2013).

The dissolution under non-sink conditions follows the trend RIV-DBA > RIV-HBA > RIV-SA > RIV-NA > RIV > RIV-IA; RIV-DBA cocrystals were much higher than the others as shown in Fig. 5. Interestingly, RIV-HBA, RIV-DBA and RIV-SA cocrystals showed an obvious "spring and parachute" pattern with a faster initial dissolution state ("spring") and a prolonged drug supersaturation state ("parachute") (Hu et al., 2019; Liu et al., 2016). After reaching the maximum drug concentration, the dissolution rate started to decrease steadily. The stable state drug concentration of RIV-HBA and RIV-SA cocrystals were close to that of pure RIV at equilibrium while the RIV-DBA showed considerably higher drug concentrations, thus indicating a higher solubility advantage. Phase and microstructure transformation is a key factor influencing the dissolution pattern (Xuan et al., 2021). The PXRD, DSC, and SEM results of residual solids after 30 min and 360 min are shown in Figs. S4, S5 and S6, respectively. For pure RIV and RIV-IA cocrystal, there were no phase and microstructures changes at 30 min or 360 min versus the initial state. However, for RIV-HBA, RIV-DBA, RIV-NA, and RIV-SA cocrystals, there were RIV precipitations after 360 min.

3.4. Intrinsic dissolution

The RIV-HBA and RIV-DBA cocrystals with higher solubility advantage were selected to perform the IDR study, and the results are shown in Fig. 6. The IDR of RIV-HBA and RIV-DBA cocrystals in pH 1.2 HCl solution at 37 °C were determined to be 0.1556 and 0.1878 mg/min/cm^2, presenting 1.94- and 2.34-fold increase versus to RIV (0.0804 mg/min/cm^2). There was no significant difference between RIV and their parent physical mixtures. The higher IDR of RIV cocrystals indicated a solubility improvement effect of cocrystals with promising chemical and physical properties rather than simple physical mixtures (Liu et al., 2020a).

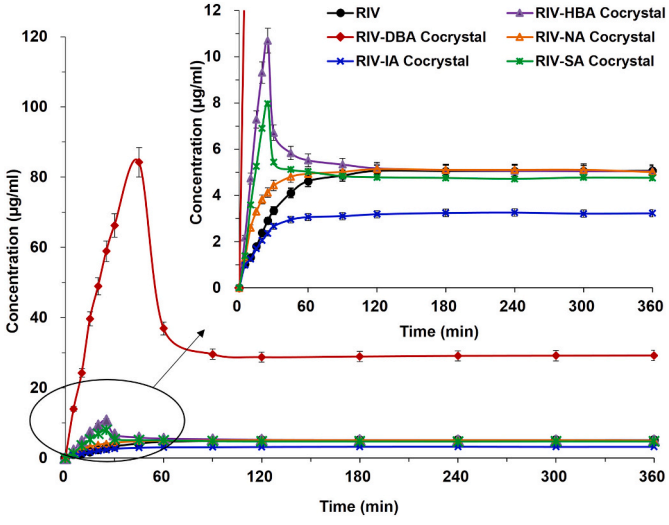

Fig. 5. Powder dissolution profiles of RIV, RIV-HBA, RIV-DBA, RIV-NA, RIV-IA, and RIV-SA cocrystals in water under non-sink conditions (mean ± SD, n = 3).

3.5. Permeation studies

3.5.1. Cytotoxicity assessment

Caco-2 cells are a stabilized, non-transformed human colon carcinoma cell line commonly used to evaluate the in vitro permeability of drugs (Tong et al., 2022). The CCK-8 method was first used to determine the cytotoxicity of RIV, PMs, and RIV cocrystals in Caco-2 cells at different concentrations. Fig. 7a shows that after 24 h of measurement, the survival rate of Caco-2 cells in the test group treated with 10, 50, 100, and 250 μg/ml was greater than 90%, thus indicating that none of the samples had toxic effects on Caco-2 cells in this concentration range. RIV concentrations of 250 μg/ml were thus selected to conduct drug transport experiments across the membrane.

3.5.2. Permeation studies

Cocrystals can improve, decrease, or have no remarkable impact on the membrane permeability of drug; the mechanisms are still unclear (Emami et al., 2018). Here, we used the epithelial cellular models (e.g., Caco-2) to conduct the permeation studies rather than commonly used Franz-type diffusion cells based on passive diffusion (Emami et al., 2018; Sanphui et al., 2015). The transport results of 250 μg/ml RIV are shown in Fig. 7b. For cocrystals, the order of P_{app} values was RIV-DBA (10.13×10^{-3} cm/min) > RIV-IA cocrystals (8.85×10^{-3} cm/min) > RIV-HBA (7.68×10^{-3} cm/min) > RIV-NA (4.50×10^{-3} cm/min) > RIV-SA (1.50×10^{-3} cm/min) cocrystals. For physical mixtures, the order of P_{app} values was RIV/NA (5.86×10^{-3} cm/min) > RIV/IA (5.38×10^{-3} cm/min) > RIV/HBA (4.54×10^{-3} cm/min) > RIV/DBA (4.52×10^{-3} cm/min) > RIV/SA (3.66×10^{-3} cm/min). Versus RIV (4.95×10^{-3} cm/min), the P_{app} values of RIV-DBA and RIV-IA cocrystals were significantly increased ($p < 0.01$) by 2.05- and 1.79-fold, respectively, thus exhibiting a cell membrane permeability enhancement effect of the two cocrystals. Moreover, the resistance value of the Caco-2 cell membrane did not change significantly before and after the experiment (Fig. S7), thus indicating that the integrity of the cell membrane did not change during the experiment. For RIV-DBA cocrystals, the improved permeability might be attributed to the enhanced solubility and the induced supersaturated state based on the interactions between the drug and coformer (Ferretti et al., 2015). The data indicated higher drug amounts across a monolayer constituted by Caco-2 cell monolayers (Tran et al., 2020). Interestingly, the permeability was also improved for RIV-IA cocrystals with low solubility, thus indicating that the solubility was not always positively related to permeability. The results were similar to previous report from Seo et al. (Seo et al., 2018), who found that cocrystals had no remarkable impact on the apical-to-basal transport rate of drug although the in vitro dissolution was enhanced. In addition, the physical mixtures had different behavior from cocrystals, which might be attributed to the formation of molecular aggregates in solution (Emami et al., 2018).

3.6. Pharmacokinetic (PK) studies in beagle dogs

Based on the results of solubility, dissolution, and monolayer cell membrane permeability studies, RIV-HBA, and RIV-DBA cocrystals with the potential to improve bioavailability were selected for further pharmacokinetic studies. The mean plasma concentration-time curves for RIV, RIV-HBA cocrystal, RIV/HBA PM, RIV-DBA cocrystal, and RIV/DBA PM in beagle dogs are shown in Fig. 8, thus illustrating the difference of RIV forms. The pharmacokinetic parameters were summarized in Table 1. The C_{max} and AUC_{0-t} of RIV-DBA cocrystal and RIV-HBA cocrystals were 677.50 ± 139.22 ng/ml and 2199.32 ± 455.95

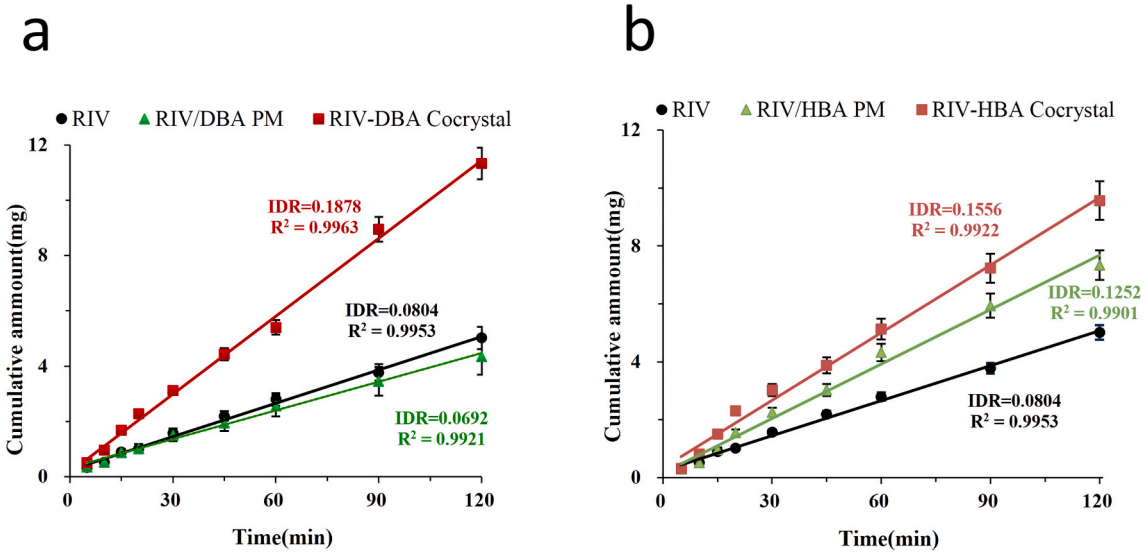

Fig. 6. Intrinsic dissolution curves of RIV-DBA(a) and RIV-HBA(b) in pH 1.2 buffer at 37 °C (mean ± SD, n = 3).

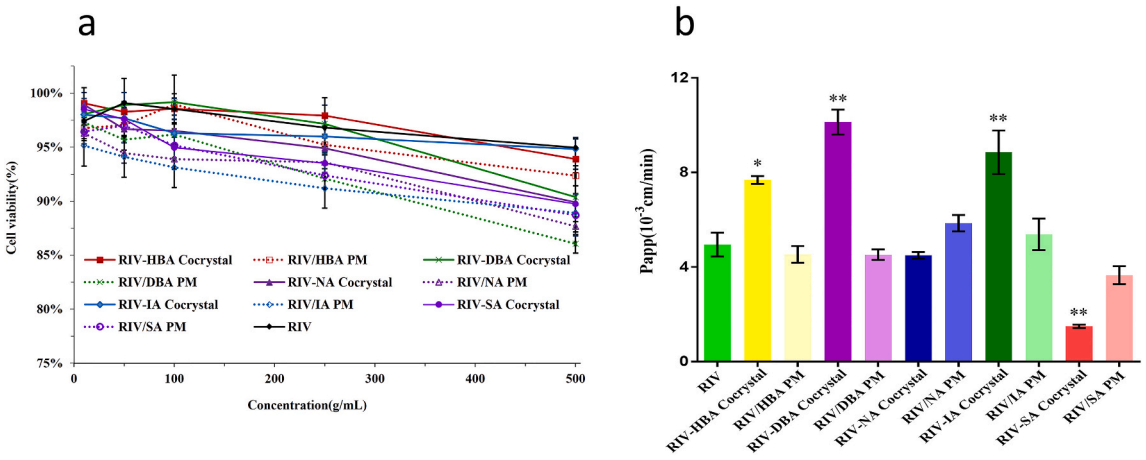

Fig. 7. (a) Results of cell cytotoxicity ($n = 6$). (b) Apparent permeability coefficients (P_{app}) of RIV, PMs, and its cocrystals across Caco-2 monolayer (n = 6). $^{*}P < 0.05$ or $^{**}P < 0.01$ compared to RIV. All the data are reported as the mean ± SD of three independent experiments.

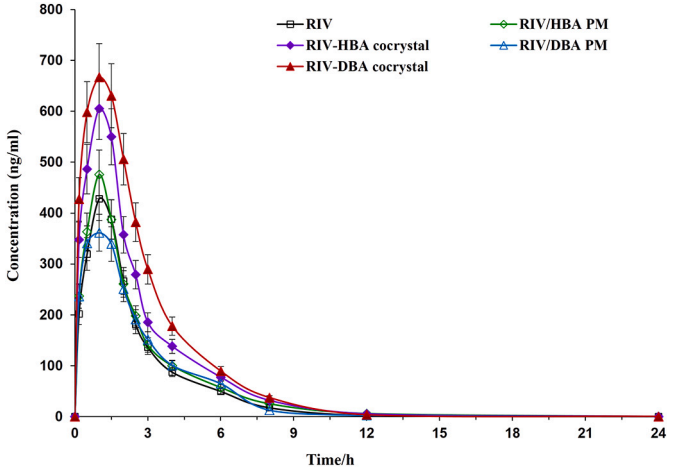

Fig. 8. Plasma concentration vs time profiles of RIV after oral administration to dogs of RIV, RIV-HBA cocrystal, RIV/HBA PM, RIV-DBA cocrystal, or RIV-DBA PMs (mean ± SD, n = 6).

Table. 1
Pharmacokinetic parameters of RIV, RIV-HBA cocrystal, RIV/HBA PM, RIV-DBA cocrystal, and RIV-DBA PMs (2 mg/kg, mean ± SD, n = 6).

Parameters	RIV	RIV/HBA PMs	RIV-HBA cocrystal	RIV/DBA PMs	RIV-DBA cocrystal
C_{max}(ng/ml)	476.51 ± 84.26	483.91 ± 77.88	623.68 ± 58.59	418.71 ± 61.19	677.50 ± 139.22
T_{max} (h)	1.08 ± 0.38	1.08 ± 0.20	1.08 ± 0.20	1.08 ± 0.38	1.17 ± 0.26
t1/2(h)	2.47 ± 0.21	2.31 ± 0.30	2.45 ± 0.39	2.33 ± 0.32	2.27 ± 0.15
MRT(h)	2.67 ± 0.28	2.98 ± 0.30	2.85 ± 0.20	2.77 ± 0.12	2.74 ± 0.15
AUC_{0-t}(ng· h/ml)	1200.27 ± 206.68	1339.09 ± 144.10	1783.49 ± 176.05	1195.32 ± 100.29	2199.32 ± 455.95
$f_{rel/\%}$	–	111.57	148.59	99.59	183.24

ng· h/ml, 623.68 ± 58.59 ng/ml and 1783.49 ± 176.05 ng· h/ml, respectively. These were both higher than raw RIV (476.51 ± 84.26 ng/ml and 1200.27 ± 206.68 ng· h/ml). The relative bioavailability (f_{rel}) of RIV-DBA cocrystal and RIV-HBA cocrystals versus raw RIV was 183.24% and 148.59%, respectively, thus indicating that the cocrystal was

successfully prepared. The f_{rel} results of RIV/HBA PMs and RIV/DBA PMs versus raw RIV showed similar bioavailability. RIV and its two cocrystals were all detected from the first blood collection point at 10 min, thus indicating a rapid absorption. The $t_{1/2}$ estimated from RIV-DBA (2.27 ± 0.15 h) and RIV-HBA (2.45 ± 0.39 h) cocrystals were similar to that of raw RIV (2.47 ± 0.21 h), but the values were statistically insignificant. The MRT_{0-t} parameters of raw RIV, RIV-DBA and RIV-HBA cocrystals were (2.67 ± 0.28 h), (2.74 ± 0.15 h), and (2.85 ± 0.20 h), respectively, which indicated that the three forms of RIV had similar action times. Overall, the higher bioavailability of RIV-DBA cocrystal and RIV-HBA cocrystal exhibited a promising perspective for further formulation development.

4. Conclusions

In the present study, cocrystals of RIV (a direct Factor Xa anticoagulant with poor water-soluble property) were prepared with p-hydroxybenzoic acid (HBA), 2,4-dihydroxybenzoic acid (DBA), nicotinamide (NA), isonicotinamide (IA), and succinic acid (SA) coformers. The solubility and dissolution behavior of the various forms of RIV, including RIV, its co-crystals, and parent physical mixtures with HBA, DBA, NA, IA, and SA were studied. The rank order of the solubility and dissolution rates of the RIV from the cocrystals were RIV-DBA > RIV-HBA > RIV-SA > RIV > RIV-NA > RIV-IA; the RIV-DBA cocrystal showed a remarkable advantage. Furthermore, RIV-DBA and RIV-IA cocrystals exhibited an increase of RIV permeability across Caco-2 cell monolayers. Pharmacokinetic studies in beagle dogs showed higher bioavailability of both RIV-HBA cocrystal and RIV-DBA cocrystal versus raw RIV. The results offer a promising strategy to improve oral delivery of RIV via enhanced bioavailability. This could benefit other poorly water-soluble BCS II category drugs with similar physical characteristics.

Declaration of Competing Interest

The authors declare that they have no known competing financial interests or personal relationships that could have appeared to influence the work reported in this paper.

Appendix A. Supplementary data

Supplementary data to this article can be found online at https://doi.org/10.1016/j.ijpx.2022.100119.

References

Abadie, B.Q., Cannon, C.P., Cavender, M.A., 2020. Novel oral anticoagulants following percutaneous coronary intervention. Circ. Cardiovasc. Interv. 13, e008465.

Al-Mallah, M.H., Sakr, S., Al-Qunaibet, A., 2018. Cardiorespiratory fitness and cardiovascular disease prevention: an update. Curr. Atheroscler. Rep. 20, 1.

Bae, J., Kim, H., Kim, W., Kim, S., Park, J., Jung, D.I., Yu, D., 2019. Therapeutic monitoring of rivaroxaban in dogs using thromboelastography and prothrombin time. J. Vet. Intern. Med. 33, 1322–1330.

Boban, A., Lambert, C., Hermans, C., 2016. Successful treatment and secondary prevention of venous thrombosis secondary to behcet disease with rivaroxaban. Case Rep. Hematol. 2016, 2164329.

Cai, L., Qin, X., Xu, Z., Song, Y., Jiang, H., Wu, Y., Ruan, H., Chen, J., 2019. Comparison of cytotoxicity evaluation of anticancer drugs between real-time cell analysis and CCK-8 method. ACS Omega 4, 12036–12042.

Cao, F., Amidon, G.L., Rodriguez-Hornedo, N., Amidon, G.E., 2016. Mechanistic analysis of cocrystal dissolution as a function of Ph and micellar solubilization. Mol. Pharm. 13, 1030–1046.

Cavanagh, K.L., Kuminek, G., Rodriguez-Hornedo, N., 2020. Cocrystal solubility advantage and dose/solubility ratio diagrams: a mechanistic approach to selecting additives and controlling dissolution-supersaturation-precipitation behavior. Mol. Pharm. 17, 4286–4301.

Childs, S.L., Kandi, P., Lingireddy, S.R., 2013. Formulation of a danazol cocrystal with controlled supersaturation plays an essential role in improving bioavailability. Mol. Pharm. 10, 3112–3127.

Cho, S., Lee, J., Yoo, Y., Cho, M., Sohn, S., Lee, B.J., 2021. Improved manufacturability and in vivo comparative pharmacokinetics of dapagliflozin cocrystals in beagle dogs and human volunteers. Pharmaceutics 13, 70.

Cysewski, P., 2018. Intermolecular interaction as a direct measure of water solubility advantage of meloxicam cocrystalized with carboxylic acids. J. Mol. Model. 24, 112.

Dalpiaz, A., Ferretti, V., Bertolasi, V., Pavan, B., Monari, A., Pastore, M., 2018. From physical mixtures to co-crystals: how the coformers can modify solubility and biological activity of carbamazepine. Mol. Pharm. 15, 268–278.

Demir, H., Gulsun, T., Ozkan, M.H., Nemutlu, E., Sahin, S., Öner, L., 2020. Assessment of dose proportionality of rivaroxaban nanocrystals. AAPS PharmSciTech 21, 228.

Elder, D.P., Holm, R., Diego, H.L., 2013. Use of pharmaceutical salts and cocrystals to address the issue of poor solubility. Int. J. Pharm. 453, 88–100.

Emami, S., Siahi-Shadbad, M., Adibkia, K., Barzegar-Jalali, M., 2018. Recent advances in improving oral drug bioavailability by cocrystals. Bioimpacts 8, 305–320.

Feng, Y., Meng, Y., Tan, F., Lv, L., Li, Z., Wang, Y., Yang, Y., Gong, W., Yang, M., 2021. Effect of surfactants and polymers on the dissolution behavior of supersaturable tecovirimat-4-hydroxybenzoic acid cocrystals. Pharmaceutics 13, 1772.

Ferretti, V., Dalpiaz, A., Bertolasi, V., Ferraro, L., Beggiato, S., Spizzo, F., Spisni, E., Pavan, B., 2015. Indomethacin co-crystals and their parent mixtures: does the intestinal barrier recognize them differently? Mol. Pharm. 12, 1501–1511.

Good, D.J., Rodríguez-Hornedo, N., 2009. Solubility advantage of pharmaceutical cocrystals. Cryst. Growth Des. 9, 2252–2264.

Grunenberg, A., Fhnrich, K., Qu Ec Kenberg, O., Reute, C., Keil, B., Gushurst, K.S., Still, E. J., 2011. Co-Crystal Compound of Rivaroxaban and Malonic Acid, EP2288606 A1.

Guo, M., Wang, K., Qiao, N., Yardley, V., Li, M., 2018. Investigating permeation behavior of flufenamic acid cocrystals using a dissolution and permeation system. Mol. Pharm. 15, 4257–4272.

Hu, C., Liu, Z., Liu, C., Li, J., Wang, Z., Xu, L., Chen, C., Fan, H., Qian, F., 2019. Enhanced oral bioavailability and anti-echinococcosis efficacy of albendazole achieved by optimizing the "Spring" and "Parachute". Mol. Pharm. 16, 4978–4986.

Kale, D.P., Ugale, B., Nagaraja, C.M., Dubey, G., Bharatam, P.V., Bansal, A.K., 2019. Molecular basis of water sorption behavior of rivaroxaban-malonic acid cocrystal. Mol. Pharm. 16, 2980–2991.

Kale, D.P., Puri, V., Kumar, A., Kumar, N., Bansal, A.K., 2020. The role of cocrystallization-mediated altered crystallographic properties on the tabletability of rivaroxaban and malonic acid. Pharmaceutics 12, 546.

Kamiloglu, S., Capanoglu, E., Grootaert, C., Van Camp, J., 2015. Anthocyanin absorption and metabolism by human intestinal Caco-2 cells—a review. Int. J. Mol. Sci. 16, 21555–21574.

Karimi-Jafari, M., Padrela, L., Walker, G.M., Croker, D.M., 2018. Creating cocrystals: a review of pharmaceutical cocrystal preparation routes and applications. Cryst. Growth Des. 18, 6370–6387.

Kushwah, V., Arora, S., Tamás Katona, M., Modhave, D., Fröhlich, E.A.-O., Paudel, A., 2021. On absorption modeling and food effect prediction of rivaroxaban, a BCS II drug orally administered as an immediate-release tablet. Pharmaceutics 13, 283.

Liu, C., Chen, Z., Chen, Y., Lu, J., Li, Y., Wang, S., Wu, G., Qian, F., 2016. Improving oral bioavailability of sorafenib by optimizing the "Spring" and "Parachute" based on molecular interaction mechanisms. Mol. Pharm. 13, 599–608.

Liu, F., Wang, L.Y., Yu, M.C., Li, Y.T., Wu, Z.Y., Yan, C.W., 2020a. A new cocrystal of isoniazid-quercetin with hepatoprotective effect: the design, structure, and in vitro/in vivo performance evaluation. Eur. J. Pharm. Sci. 144, 105216.

Liu, L., Zou, D., Zhang, Y., Zhang, Q., Feng, Y., Guo, Y., Liu, Y., Zhang, X., Cheng, G., Wang, C., Zhang, Y., Zhang, L., Wu, L., Chang, L., Su, X., Duan, Y., Zhang, Y., Liu, M., 2020b. Pharmaceutical salts/cocrystals of enoxacin with dicarboxylic acids: Enhancing in vitro antibacterial activity of enoxacin by improving the solubility and permeability. Eur. J. Pharm. Biopharm. 154, 62–73.

Metre, S., Mukesh, S., Samal, S.K., Chand, M., Sangamwar, A.T., 2018. Enhanced biopharmaceutical performance of rivaroxaban through polymeric amorphous solid dispersion. Mol. Pharm. 15, 652–668.

Ruiz-Morales, Y., Romero-Martinez, A., 2018. Coarse-grain molecular dynamics simulations to investigate the bulk viscosity and critical micelle concentration of the ionic surfactant sodium dodecyl sulfate (SDS) in aqueous solution. J. Phys. Chem. B 122, 3931–3943.

Sanphui, P., Devi, V.K., Clara, D., Malviya, N., Ganguly, S., Desiraju, G.R., 2015. Cocrystals of hydrochlorothiazide: solubility and diffusion/permeability enhancements through drug-coformer interactions. Mol. Pharm. 12, 1615–1622.

Sathisaran, I., Dalvi, S.V., 2018. Engineering cocrystals of poorlywater-soluble drugs to enhance dissolution in aqueous medium. Pharmaceutics 10, 108.

Seo, J.W., Hwang, K.M., Lee, S.H., Kim, D.W., Park, E.S., 2018. Preparation and characterization of adefovir dipivoxil-stearic acid cocrystal with enhanced physicochemical properties. Pharm. Dev. Technol. 23, 890–899.

Takács-Novák, K., Szőke, V., Völgyi, G., Horváth, P., Ambrus, R., Szabó-Révész, P., 2013. Biorelevant solubility of poorly soluble drugs: Rivaroxaban, furosemide, papaverine and niflumic acid. J. Pharm. Biomed. Anal. 83, 279–285.

Tian, F., Sandler, N., Gordon, K.C., McGoverin, C.M., Reay, A., Strachan, C.J., Saville, D. J., Rades, T., 2006. Visualizing the conversion of carbamazepine in aqueous suspension with and without the presence of excipients: a single crystal study using SEM and Raman microscopy. Eur. J. Pharm. Biopharm. 64, 326–335.

Tong, M., Wu, X., Zhang, S., Hua, D., Li, S., Yu, X., Wang, J., Zhang, Z., 2022. Application of TPGS as an efflux inhibitor and a plasticizer in baicalein solid dispersion. Eur. J. Pharm. Sci. 168, 106071.

Tran, V.N., Viktorova, J., Ruml, T., 2020. Mycotoxins: biotransformation and bioavailability assessment using Caco-2 cell monolayer. Toxins (Basel) 12, 628.

Wallace, C.J., Medina, S.H., ElSayed, M.E., 2014. Effect of rhamnolipids on permeability across Caco-2 cell monolayers. Pharm. Res. 31, 887–894.

Weitz, J.I., Bauersachs, R., Becker, B., Berkowitz, S.D., Freitas, M.C.S., Lassen, M.R., Metzig, C., Raskob, G.E., 2020. Effect of osocimab in preventing venous thromboembolism among patients undergoing knee arthroplasty: the FOXTROT randomized clinical trial. JAMA 323, 130–139.

Wen, H., Morris, K.R., Park, K., 2005. Hydrogen bonding interactions between adsorbed polymer molecules and crystal surface of acetaminophen. J. Colloid Interface Sci. 290, 325–335.
Wingert, N.R., Dos Santos, N.O., Campanharo, S.C., Jablonski, A., Steppe, M., 2018. Quantitative assessment of poorly soluble anticoagulant rivaroxaban by microemulsion electrokinetic chromatography. J. Chromatogr. Sci. 56, 650–655.
Wong, S.N., Chen, Y.C.S., Xuan, B., Sun, C.C., Chow, S.F., 2021. Cocrystal engineering of pharmaceutical solids: therapeutic potential and challenges. CrystEngComm 23, 7005–7038.
Xuan, B., Chen, Y.C.S., Wong, K.C., Chen, R., Lo, P.S., Lakerveld, R., Tong, H.H.Y., Chow, S.F., 2021. Impact of cocrystal solution-state stability on cocrystal dissociation and polymorphic drug recrystallization during dissolution. Int. J. Pharm. 610, 121239.
Xue, X., Cao, M., Ren, L., Qian, Y., Chen, G., 2018. Preparation and optimization of rivaroxaban by Self-Nanoemulsifying Drug Delivery System (SNEDDS) for enhanced Oral bioavailability and no food effect. AAPS PharmSciTech 19, 1847–1859.
Yang, Z., Yang, Y., Xia, M., Dai, W., Zhu, B., Mei, X., 2022. Improving the dissolution behaviors and bioavailability of abiraterone acetate via multicomponent crystal forms. Int. J. Pharm. 614, 121460.
Young, G., Lensing, A.W.A., Monagle, P., Male, C., Thelen, K., Willmann, S., Palumbo, J. S., Kumar, R., Nurmeev, I., Hege, K., Bajolle, F., Connor, P., Hooimeijer, H.L., Torres, M., Chan, A.K.C., Kenet, G., Holzhauer, S., Santamaria, A., Amedro, P., Beyer-Westendorf, J., Martinelli, I., Massicotte, M.P., Smith, W.T., Berkowitz, S.D., Schmidt, S., Price, V., Prins, M.H., Kubitza, D., Investigators, E.I.-J.P., 2020. Rivaroxaban for treatment of pediatric venous thromboembolism. An Einstein-Jr phase 3 dose-exposure-response evaluation. J. Thromb. Haemost. 18, 1672–1685.
Zhou, J., Li, L., Zhang, H., Xu, J., Huang, D., Gong, N., Han, W., Yang, X., Zhou, Z., 2020. Crystal structures, dissolution and pharmacokinetic study on a novel phosphodiesterase-4 inhibitor chlorbipram cocrystals. Int. J. Pharm. 576, 118984.